

Collapse dynamics of dry granular columns: From free-fall to quasistatic flowWladimir Sarlin^{1,*}, Cyprien Morize^{1,†}, Alban Sauret², and Philippe Gondret¹¹Université Paris-Saclay, CNRS, Laboratoire FAST, F-91405 Orsay, France²Department of Mechanical Engineering, University of California, Santa Barbara, California 93106, USA

(Received 24 September 2021; accepted 7 December 2021; published 23 December 2021)

Gravity-driven collapses involving large amounts of dense granular material, such as landslides, avalanches, or rock falls, in a geophysical context, represent significant natural hazards. Understanding their complex dynamics is hence a key concern for risk assessment. In the present work, we report experiments on the collapse of quasi-two-dimensional dry granular columns under the effect of gravity, where both the velocity at which the grains are released and the aspect ratio of the column are varied to investigate the dynamics of the falling grains. At high release velocity, classical power laws for the final deposit are recovered, meaning those are representative of a free-fall-like regime. For sufficiently high aspect ratios, the top of the column undergoes an overall free-fall-like motion. In addition, for all experiments, the falling grains also spread horizontally in a free-fall-like motion, and the characteristic time of spreading is related to the horizontal extension reached by the deposit at all altitudes. At low release velocity, a quasistatic state is observed, with scaling laws for the final geometry identical to those of the viscous regime of granular-fluid flow. The velocity at which the grains are released governs the collapse dynamics. Between these two asymptotic regimes, higher release velocity correlates with smaller impact on the collapse dynamics. The criterion $\bar{V} \geq 0.4\sqrt{gH_0}$, where H_0 is the initial height of the column, is found for the mean release velocity \bar{V} not to influence the granular collapse.

DOI: [10.1103/PhysRevE.104.064904](https://doi.org/10.1103/PhysRevE.104.064904)**I. INTRODUCTION**

Geophysical gravity-driven flows such as landslides and avalanches are as fascinating as they are complex due to their inherent unsteadiness and the large deformation experienced by the flowing mass during its motion. Understanding these phenomena is of great interest as they pose serious threats to human activity in mountainous areas [1].

A common approach to characterize these flows at the laboratory scale consists in using granular materials to mimic the slumping mass. In particular, the collapse of a column of grains is a simple but relevant configuration for modeling landslides [2], so that it has been extensively studied in the past two decades [3–31]. The aim of these studies was to reach a better understanding of such flows and describe the final morphology of the deposits. The usual experimental configuration consists of a column of granular material of height H_0 and initial width L_0 (two-dimensional setup [4]) or radius R_0 (axisymmetric setup [5]), initially at rest. When the column is released, the grains fall and spread over the ground. The initial aspect ratio of the column, defined as $a = H_0/L_0$, was found to govern the final geometry of the deposits. The influence of a on the final height H_f and run-out length $\Delta L_f = L_f - L_0$ has been captured through power laws both for the rectangular [4,6] and the axisymmetric [3,5] geometries. For instance, Lajeunesse *et al.* [4] found that for glass beads in a rectangular channel the relative run-out distance $\Delta L_f/L_0$ was proportional to a when $a \lesssim 3$ and to $a^{2/3}$ when $a \gtrsim 3$, while the relative final height H_f/L_0 was equal to a for $a \lesssim 0.7$ and proportional

to $a^{1/3}$ at higher aspect ratios. In the axisymmetric configuration, different scaling laws have been obtained [3–5].

Numerical simulations reproduced these scalings for the final geometry using contact dynamics algorithms [7], shallow water equations [11], and/or continuum approaches [16,24] implementing pressure-dependent granular rheologies such as the $\mu(I)$ rheology introduced by Jop *et al.* [32]. The numerical values of the prefactors, exponents, and critical aspect ratios of these power laws slightly vary among authors [4,6–8,25,27]. In particular, the exponents were shown to be independent of the material properties, which only affect the numerical prefactors [8,12,29]. However, despite extensive work, no clear explanation exists to rationalize these scalings.

Experiments conducted by Mériaux [10] addressed the case where inertia is negligible in the problem, i.e., when the granular column is slowly released using a horizontally moving gate. In this situation, empirical scalings are again obtained, which differ from those obtained when the column is instantaneously released [7]. In a different context, the collapse of a liquid-immersed granular column was investigated both experimentally [17,26,30,31] and numerically [19,25,31]. In this case, the collapse dynamics depends not only on the aspect ratio a of the column but also on the density ratio between the granular medium and the surrounding fluid, and the Stokes number, which compares the grain inertia to the viscous fluid forces. In particular, the viscous regime, at low Stokes number, is characterized by the absence of grain inertia [26].

Nevertheless, whereas extensive efforts were made to investigate the behavior of the run-out distance at the base of the column, there is a lack of experimental investigations focusing on the overall dynamics of the collapse. In the present work, the granular slumping dynamics is investigated in detail

*wladimir.sarlin1@universite-paris-saclay.fr

†cyprien.morize@universite-paris-saclay.fr

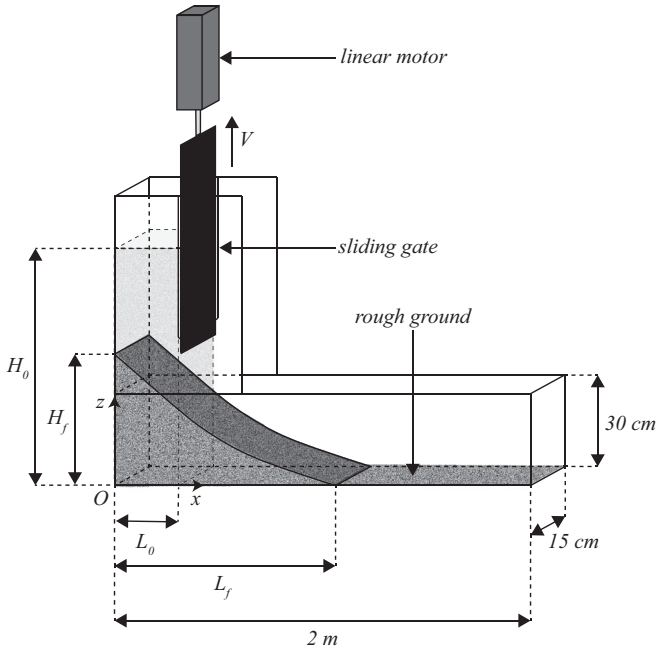


FIG. 1. Sketch of the experimental setup, showing the initial rectangular granular column of height H_0 and width L_0 , and a schematic view of the final deposit of height H_f and run-out length L_f .

by varying the velocity at which the grains are released for different aspect ratios of the initial granular column. The experimental setup is first described in Sec. II. In Sec. III, the different regimes observed depending on the release velocity are characterized qualitatively. Quantitative results are discussed in Sec. IV, where we describe both the dynamics at high and low release velocities as well as the transition between these two asymptotic regimes.

II. EXPERIMENTAL SETUP

The experiments were conducted using the setup presented in Fig. 1. On the left side of a $2 \times 0.15 \times 0.3$ m parallelepipedic glass tank, a column of granular material is initially retained by a sliding vertical gate, located at a distance L_0 from the left wall. The x axis is along the horizontal direction, while the z axis is along the vertical one. The origin is located at the bottom left end of the experimental setup. A flat rough ground, made with the same grains as the granular column, covers the bottom of the tank to ensure a no-slip boundary condition. To avoid possible segregation effects due to polydispersity [21], we used monodisperse glass beads of diameter $d \simeq 5$ mm and density $\rho \simeq 2.5$ g/cm³, with a measured packing fraction $\phi \simeq 0.64$. Besides, the angle of repose θ_r was measured at about $23.5 \pm 1.2^\circ$, in agreement with previous studies [4,33]. The spanwise dimension of the channel was chosen large enough to prevent confinement effects [34]. It was indeed verified that a channel width greater than 10 cm, corresponding to $20d$, ensures no significant influence of the sidewalls on the granular collapse [35] (see Fig. 2.18 therein).

At $t = 0$, the gate is lifted using a brushless servomotor so that the column collapses and spreads under the effect of

TABLE I. Experimental parameters considered in this study: height H_0 , width L_0 , and aspect ratio a of the initial granular column, and nominal release velocity V of the sliding gate.

	H_0 (cm)	L_0 (cm)	a	V (m/s)
A	[10 - 50]	[2.5 - 20]	[0.5 - 20]	1.2
B	[6 - 45]	[7.5 - 20]	[0.3 - 6]	1.0×10^{-2}
C	15	20	0.75	$[1.0 \times 10^{-3} - 1.2]$
D	20	10	2	$[1.0 \times 10^{-2} - 1.2]$
E	37.5	7.5	5	$[1.0 \times 10^{-3} - 1.2]$

gravity. Using a motor allows controlling the nominal velocity V at which the column is released. Across experiments, this release velocity was varied over three decades, namely from 1 mm s^{-1} to 1.2 m s^{-1} , for different initial aspect ratios of the column.

The parameters considered in this study are reported in Table I, and are divided into five series. The experiments conducted at high release velocity ($V = 1.2 \text{ m s}^{-1}$) are gathered in series A, while experiments performed at a low release velocity ($V = 1 \text{ cm s}^{-1}$) are collected in series B. Finally, the transition between these two limits was investigated in series C, D, and E, each corresponding to a fixed aspect ratio a of 0.75, 2, and 5, respectively. The corresponding values for H_0 and L_0 are also reported in Table I.

The collapse dynamics is recorded from the sidewall of the tank using a Nikon D3300 camera, operating at 50 Hz. Image sequences are then processed to obtain the time evolution of the granular contour using a custom-made MATLAB routine based on a thresholding method.

III. PHENOMENOLOGY

Different collapse dynamics and geometries of the final deposit are observed when varying the release velocity. Two asymptotic behaviors can be highlighted for high and low values of V . In the first situation, corresponding to the experiments conducted at high release velocity (series A), the classical granular collapse is observed, as previously reported in the literature [4,6,7]. The grains quickly fall and spread over the ground with high inertia, as illustrated in Figs. 2(a)–2(f) for a column with a high aspect ratio ($a = 5$) and, to a lesser extent, in Figs. 3(a)–3(e) in the case of a low aspect ratio ($a = 0.5$). While the bottom of the column mainly follows a horizontal motion [Figs. 2(c) and 3(c)], its top seems to undergo a vertical acceleration for sufficiently high aspect ratios ($a \gtrsim 3$) [top of the column in Figs. 2(b) and 2(c)]. This behavior was identified as the free-fall regime by Staron and Hinch [7]. The overall motion presents strong unsteadiness and leads to a final geometry that exhibits a significant curvature of the deposit, especially at large aspect ratio [Fig. 2(f)].

The experiments conducted at low release velocity (series B) show a very different behavior, as can be seen in Figs. 2(g)–2(l) and 3(f)–3(j). A quasistatic flow occurs, and at all times the moving granular contour is roughly triangular, with a foot angle close to the angle of repose θ_r of the material. Only minor deviations from a triangular shape are observed, especially at the onset of the granular slide, as illustrated by the slightly curved interface in Figs. 2(h)–2(j). In that respect, the

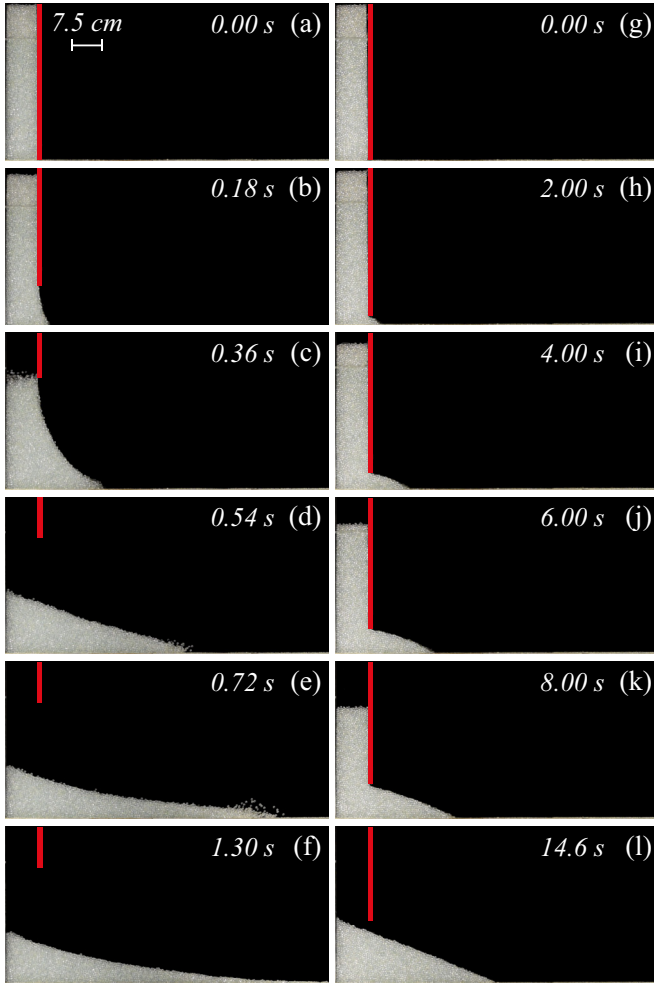


FIG. 2. Image sequences of the collapse of a rectangular granular column with $H_0 = 37.5$ cm and $L_0 = 7.5$ cm ($a = 5$) [(a)–(f)] for high release velocity ($V = 1.2$ m s $^{-1}$), and [(g)–(l)] for low release velocity ($V = 0.01$ m s $^{-1}$). The red thick line indicates the location of the sliding gate.

final morphology of the deposit has no significant curvature at the end of the collapse, and for sufficiently large aspect ratios ($a \gtrsim 0.8$) it exhibits a triangular shape, as illustrated in Fig. 2(l). At a given aspect ratio, the run-out distance is systematically larger for experiments at large release velocity, while the final height is higher for experiments at low release velocity. For sufficiently low aspect ratios ($a \lesssim 0.8$), a trapezoidal shape is observed for the final deposit as can be seen in Fig. 3(j), since only a fraction of the initial column collapses. In that case, the run-out distance is again larger for the experiments at large release velocity, while the final height systematically coincides with the initial one.

Between these two asymptotic situations of high and low release velocity, a transition regime is observed: For a given value of a , when the release velocity is increased, the run-out distance and the curvature of the final deposit surface increase, while the final height decreases (when $a \gtrsim 0.8$) or stays constant (for $a \lesssim 0.8$).

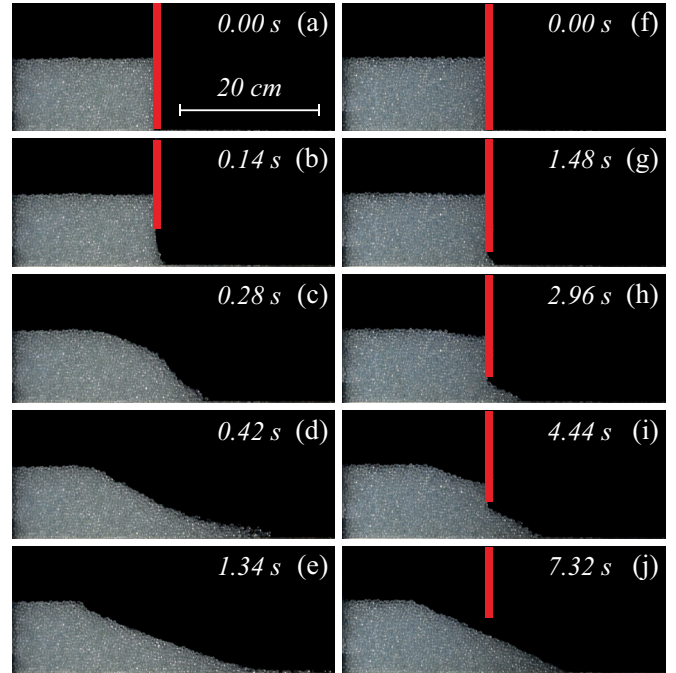


FIG. 3. Image sequences of the collapse of a rectangular granular column with $H_0 = 10$ cm and $L_0 = 20$ cm ($a = 0.5$) [(a)–(e)] for high release velocity ($V = 1.2$ m s $^{-1}$) and [(f)–(j)] for low release velocity ($V = 0.01$ m s $^{-1}$). The red thick line indicates the location of the sliding gate.

IV. RESULTS AND DISCUSSION

A. Free-fall regime

The final height H_f and run-out distance $\Delta L_f = L_f - L_0$ of the deposit (with H_f and L_f defined as in Fig. 1) are systematically determined for each experiment. It should be pointed out that L_f is actually evaluated at $z = d$, i.e., at one grain diameter from the bottom plate, to reduce measurement uncertainties. The evolution of the relative final height H_f/L_0 and run-out distance $\Delta L_f/L_0$ with the initial aspect ratio is presented in Figs. 4(a) and 4(b), respectively, for the experiments at large release velocity (\star). In addition, the following fits, inspired by Lajeunesse *et al.* [4], for the relative run-out distance,

$$\frac{\Delta L_f}{L_0} \simeq \begin{cases} 1.85 a & \text{for } a \lesssim 3, \\ 2.67 a^{2/3} & \text{for } a \gtrsim 3, \end{cases} \quad (1)$$

and final height,

$$\frac{H_f}{L_0} \simeq \begin{cases} a & \text{for } a \lesssim 0.8, \\ 0.93 a^{1/3} & \text{for } a \gtrsim 0.8. \end{cases} \quad (2)$$

are also reported (black dashed lines). An excellent agreement is observed between the experimental data obtained at high release velocities and the scaling laws given by (1) and (2).

To investigate in more detail the dynamics of the collapse, we observe the time evolution of the height $H(x, t)$ for different values of x , between 0 and L_0 . In addition, the time evolution of the spreading length $L(z, t)$ is also extracted at different altitudes z , between 0 and H_f , for all aspect ratios considered in this study. An example of the time evolution

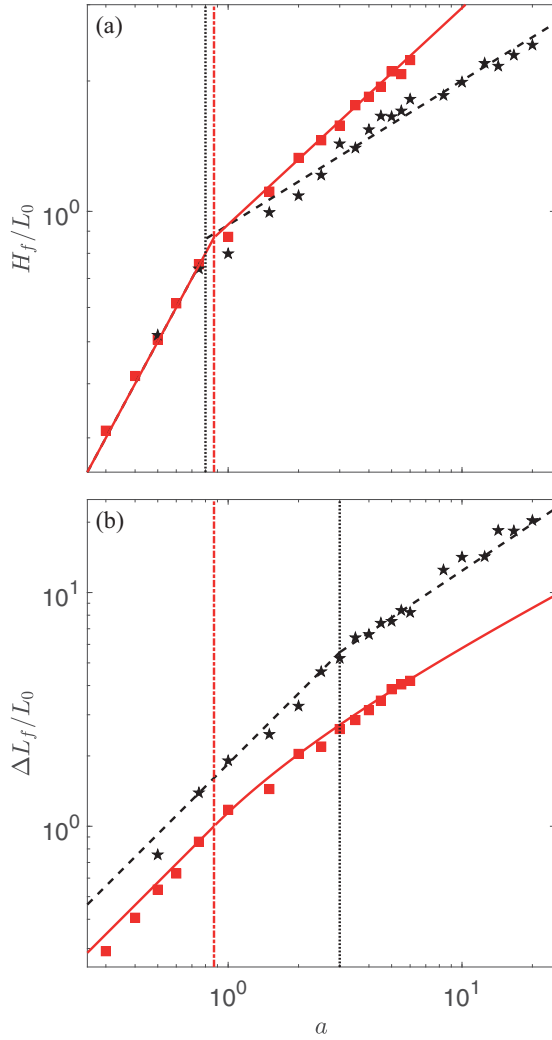


FIG. 4. Evolution of (a) the relative final height H_f/L_0 and (b) the relative run-out distance $\Delta L_f/L_0$ of the deposits as a function of the initial aspect ratio a of the column. (\star) Data from series A; (\blacksquare) data from series B; (---) power laws from Eqs. (1) and (2); (—) Eqs. (10a), (10b), (11a), and (11b), with $\theta_r = 23.5^\circ$; (⋯⋯) critical aspect ratios of the free-fall regime (a) $a \simeq 0.8$ and (b) $a \simeq 3$ from Eqs. (1) and (2), respectively; and (-·-·) critical aspect ratio of the quasistatic regime $a_{cr} \simeq 0.87$, as defined in Eq. (12).

of these parameters is reported in Figs. 5(a)–5(b), for an initial column with $H_0 = 37.5$ cm and $L_0 = 7.5$ cm ($a = 5$). In Fig. 5(a), $H(x, t)$ is plotted as a function of $t - t_{0z}$, where t_{0z} corresponds to the time for which a vertical displacement greater than $1.5d$ is detected. $H(x, t)$ decreases from H_0 to a final height $H_f(x)$, as presented in Fig. 5(a) for ten equally spaced values of x between 0 and L_0 . An acceleration phase, followed by a deceleration stage, is observed. During the acceleration period, all experimental data collapse on a master curve, whose equation corresponds to a free-fall-like motion,

$$H(x, t) \simeq H_0 - \frac{1}{2}\alpha g(t - t_{0z})^2, \quad (3)$$

where $\alpha \simeq 0.56$. As illustrated in Fig. 5(a), the different curves depart from this law of motion when the deceleration stage of the collapse occurs, here around 0.25 s. This separation happens at a slightly different time for each curve and

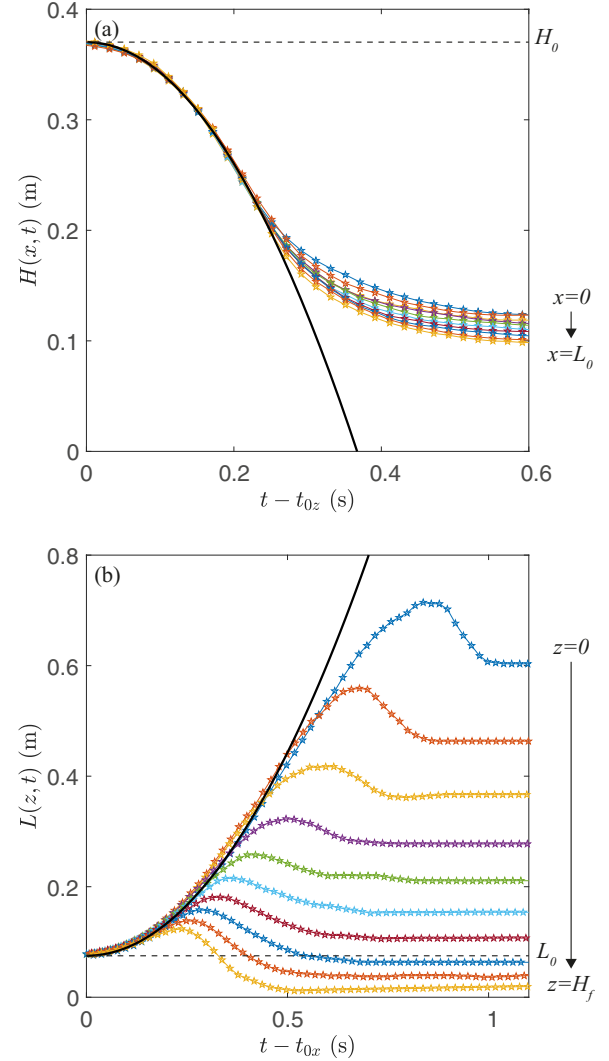


FIG. 5. Example of the time evolution of (a) the height $H(x, t)$ and (b) the spreading length $L(z, t)$ of the collapse, for an initial column of height $H_0 = 37.5$ cm and width $L_0 = 7.5$ cm ($a = 5$). The different curves correspond to ten equally spaced values of (a) x between 0 and L_0 (from top to bottom) and (b) z between 0 and H_f (from top to bottom). The thick lines show Eq. (3) in panel (a) and Eq. (4) in panel (b).

leads to different final heights depending on the considered value of x .

In Fig. 5(b), the spreading length $L(z, t)$ is plotted, for ten equally spaced altitudes between 0 and H_f , as a function of $t - t_{0x}$, where t_{0x} is the time at which the bottom of the sliding gate reaches z , which allows initiating the spreading at this altitude. At each value of z , $L(z, t)$ also exhibits an acceleration phase, followed by a deceleration. At the end of the deceleration stage, $L(z, t)$ reaches an asymptotic value $L_f(z)$, after passing through a maximum value.

The acceleration phases at all altitudes also seem to collapse on a master curve, which is found to be proportional to a free-fall-like motion,

$$L(z, t) \simeq L_0 + \frac{1}{2}\beta g(t - t_{0x})^2, \quad (4)$$

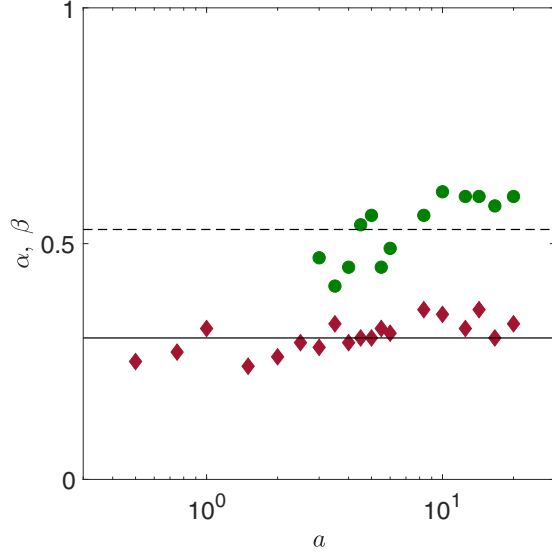


FIG. 6. Evolution of the coefficients (●) α and (◆) β with the aspect ratio a , at high release velocity. Mean values (---) $\bar{\alpha} = 0.53$ and (—) $\bar{\beta} = 0.30$ are also indicated.

with $\beta \simeq 0.30$. The experimental curves deviate from Eq. (4) earlier at larger altitude, revealing that the acceleration stage of the spreading is getting shorter for increasing values of z .

The evolution of the coefficients α and β with the aspect ratio of the column a is reported in Fig. 6 for all experiments at large release velocity, i.e., of series A. It is important to note that there is no available values for α as soon as $a \lesssim 3$, as it was not possible to distinguish experimentally a clear acceleration stage, such as the one presented in Fig. 5(a), for these low aspect ratios. This observation is in agreement with results from previous numerical simulations [7,25], which showed that the free fall of the top of the column only occurred when $a \gtrsim 2.5$. Despite some scattering of the data, the β values are significantly lower than the α values. There is no significant influence of the aspect ratio on β , as all experiments are close to a mean value $\bar{\beta} \simeq 0.30 \pm 0.06$. For the coefficient α , it can be noticed that values when $a \lesssim 8$ are slightly below those obtained at higher aspect ratios, which saturate at a value close to 0.6. However, at first order, all values are roughly distributed around a mean value $\bar{\alpha} \simeq 0.53 \pm 0.12$. This value, smaller than one, slightly differs from past numerical results of Staron and Hinch [7] and Jing *et al.* [25], but also from the experimental work of Balmforth and Kerswell [8]. It could be an indication that the material properties as well as the boundary conditions at the sidewalls may have a significant influence on α and β .

These observations can be summarized briefly as follows: The top of the column uniformly undergoes a free-fall-like motion at an acceleration of about $0.5g$ as soon as $a \gtrsim 3$, while the column spreads laterally, also in a free-fall-like motion at a typical acceleration of about $0.3g$, for all aspect ratios considered in this study.

To further confirm this free-fall-like dynamics, two characteristic times are systematically extracted from the $H(x, t)$ and $L(z, t)$ curves: The characteristic times of vertical fall $\tau_z(x)$ and of horizontal spreading $\tau_x(z)$ are taken as the times at

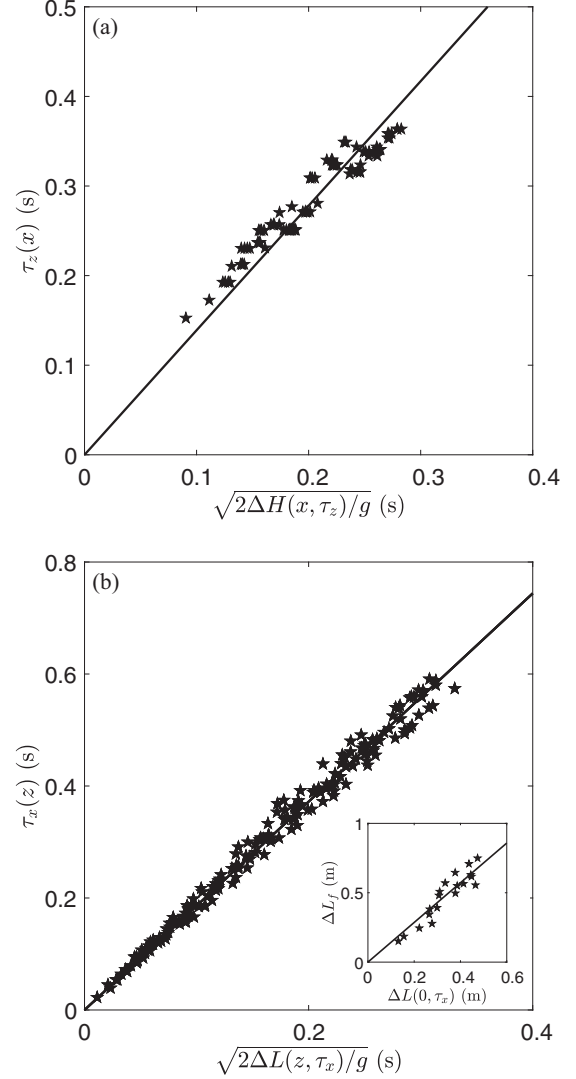


FIG. 7. (a) Evolution of $\tau_z(x)$ with $\sqrt{2\Delta H(x, \tau_z)/g}$. (★) All experiments where $a \gtrsim 3$, with different initial aspect ratios a and at different positions x from the left wall. The solid line (—) is the best linear fit of slope 1.39. (b) Evolution of $\tau_x(z)$ with $\sqrt{2\Delta L(z, \tau_x)/g}$. (★) All experiments, for different aspect ratios a and at different heights z from the bottom. The solid line (—) is the best linear fit of slope 1.86. The inset shows the comparison between the final run-out distance ΔL_f and the typical spreading length $\Delta L(0, \tau_x)$ at the base of the column at time $\tau_x(0)$, with (—) being the best linear fit of slope 1.43.

which $H(x, t)$ and $L(z, t)$ deviate by more than 10% (i.e., out of the error range) from Eqs. (3) and (4), respectively.

For all experiments at large release velocity (series A), Figs. 7(a) and 7(b) show these characteristic times $\tau_z(x)$ and $\tau_x(z)$ as functions of the typical free-fall times $\sqrt{2\Delta H(x, \tau_z)/g}$, where $\Delta H(x, \tau_z) = H_0 - H(x, \tau_z)$, and $\sqrt{2\Delta L(z, \tau_x)/g}$, where $\Delta L(z, \tau_x) = L(z, \tau_x) - L_0$, respectively, at all values of x (resp. z) considered. The best fit of the data from Fig. 7(a) leads to

$$\tau_z(x) \simeq 1.39 \sqrt{2\Delta H(x, \tau_z)/g}, \quad (5)$$

where the prefactor is very close to $1/\sqrt{\alpha} \simeq 1.37$. This confirms that for tall columns the time of collapse $\tau_z(x)$ is proportional to the free-fall time over the typical variation in height $\Delta H(x, \tau_z)$. We should emphasize again that this free-fall-like motion of the top of the column is absent for low aspect ratios ($a \lesssim 3$). In addition, Fig. 7(b) shows that the relation

$$\tau_x(z) \simeq 1.86\sqrt{2\Delta L(z, \tau_x)/g}, \quad (6)$$

fits well the data, with a prefactor again in agreement with the value $1/\sqrt{\beta} \simeq 1.82$, which means that the characteristic time of spreading $\tau_x(z)$ at an altitude z is also proportional to the free-fall like time over the corresponding typical lateral extension $\Delta L(z, \tau_x)$. Moreover, the inset in figure 7(b) compares the final run-out distance ΔL_f to the spreading length $\Delta L(0, \tau_x)$ at the base of the column at time $\tau_x(0)$. It should be pointed out that here again $\Delta L(0, \tau_x)$ and $\tau_x(0)$ are evaluated at $z = d$ to reduce measurement uncertainties. A linear relation of slope 1.43 can be inferred between the two characteristic lengths. Using this observation, we obtain from Eq. (6) the following scaling for the time of collapse at the base of the column:

$$\tau_x(0) \propto \sqrt{2\Delta L_f/g}. \quad (7)$$

In addition, considering the expressions provided by Eq. (1) for the run-out length ΔL_f , we obtain

$$\tau_x(0) \propto \begin{cases} \sqrt{2H_0/g} & \text{for } a \lesssim 3, \\ a^{-1/6}\sqrt{2H_0/g} & \text{for } a \gtrsim 3. \end{cases} \quad (8)$$

Hence, for low aspect ratios ($a \lesssim 3$), the characteristic time of spreading should be proportional to the free-fall time $\sqrt{2H_0/g}$ over the initial height H_0 , in agreement with the findings of Lajeunesse *et al.* [4]. However, there should also be a subtle influence of a on the spreading time for high aspect ratios ($a \gtrsim 3$), which could explain the behavior reported by Lacaze *et al.* [14] (see Fig. 8 therein).

The characteristic spreading time at the bottom of the column, $\tau_x(0)$, normalized by $\sqrt{2H_0/g}$, is shown as a function of the aspect ratio in a log-log representation in Fig. 8. A quite good agreement is observed with the scalings of Eq. (8), despite some scattering. In particular, a plateau value of about 2.3 is obtained, for a lower than a critical value comprised between 2 and 3, while a slight decrease, beyond the error range, occurs at larger values of a , which is compatible with a power law of exponent $-1/6$. These observations highlight the influence of the aspect ratio of the column on the characteristic time of the granular spreading.

B. Quasistatic regime

For a low release velocity of the granular column, i.e., corresponding to the experiments of series B, the inertia of the grains is negligible, so that the granular slide exhibits a quasistatic evolution. In Figs. 4(a) and 4(b), the relative final height H_f/L_0 and run-out distance $\Delta L_f/L_0$ are shown for these experiments (■), with both parameters presenting a strict growth with the initial aspect ratio of the column. In Fig. 4(a), the relative final height is found to either coincide (when $a \lesssim 0.9$) or be higher (for $a \gtrsim 0.9$) than the values

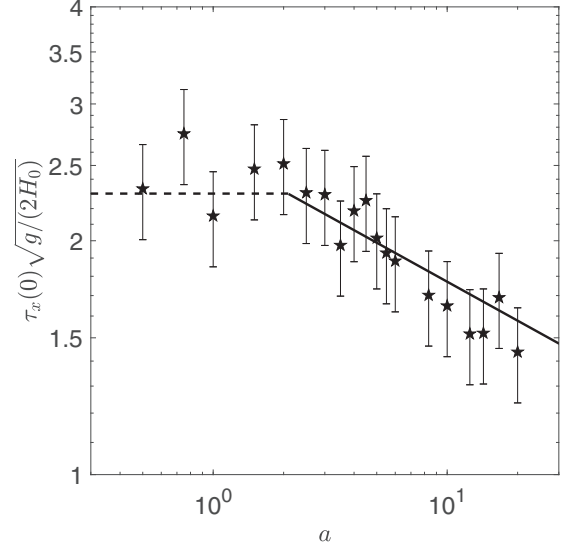


FIG. 8. Evolution of the relative characteristic time of spreading at the base of the column $\tau_x(0)\sqrt{g/(2H_0)}$ as a function of the aspect ratio a . (★, with error bars) experimental data; (—) $\tau_x(0) = 2.3\sqrt{2H_0/g}$; and (—) $\tau_x(0) = 2.6a^{-1/6}\sqrt{2H_0/g}$.

obtained at large release velocity (series A). In Fig. 4(b), the run-out distance obtained for experiments at low release velocity is systematically lower than for experiments at large release velocity. As already mentioned in Sec. III, a triangular shape with a straight slope is obtained experimentally for sufficiently high aspect ratios ($a \gtrsim 0.9$), as observed in Fig. 2(i). Considering the conservation of mass and that the final geometry is described by the angle of repose θ_r of the granular material leads to

$$H_0L_0 = \frac{H_fL_f}{2}, \quad (9a)$$

$$\frac{H_f}{L_f} = \tan \theta_r. \quad (9b)$$

Solving Eq. (9) in terms of H_f and L_f leads to the following expressions:

$$\frac{H_f}{L_0} = \sqrt{2a \tan \theta_r}, \quad (10a)$$

$$\frac{\Delta L_f}{L_0} = \sqrt{\frac{2a}{\tan \theta_r}} - 1. \quad (10b)$$

In contrast, for sufficiently low aspect ratios, namely when $a \lesssim 0.9$, a trapezoidal shape is obtained, as part of the initial column remains at rest during the collapse [see Fig. 3(j)]. Hence, using once again mass conservation and the fact that in this case $H_f = H_0$, we obtain the following relations:

$$\frac{H_f}{L_0} = a, \quad (11a)$$

$$\frac{\Delta L_f}{L_0} = \frac{a}{2 \tan \theta_r}. \quad (11b)$$

The critical aspect ratio a_c , which separates the triangular shape regime from the trapezoidal one, is straightforwardly

derived from the equality of Eqs. (10a) and (11a):

$$a_c = 2 \tan \theta_r. \quad (12)$$

The predictions given by Eqs. (10a), (10b), (11a), and (11b) are reported in Fig. 4. An excellent agreement is obtained between these scalings and experiments made at low release velocity, for $\theta_r = 23.5^\circ$. This value of θ_r is consistent with the measured angle of repose of the spherical glass beads used in the present study. It also gives the following estimate for the critical aspect ratio: $a_c \simeq 0.87$, which corresponds quantitatively to the observed transition between trapezoidal and triangular shapes around 0.9.

It should be mentioned that these scalings for the quasistatic regime are identical to those obtained by Rondon *et al.* [17], and by Bougouin and Lacaze [26], for the collapse of an initially dense granular column in a viscous fluid. This is not surprising, as inertia is also negligible in the viscous regime, so that here again the collapse is quasistatic and the final morphology is governed by the angle of repose of the material. It is also in very good quantitative agreement with the results of Mériaux for the geometry of the deposits [10]. Indeed, Mériaux studied the quasistatic collapse of a granular column when the retaining wall is slowly removed horizontally. In the case of glass beads with a diameter between 600 and 850 μm , the relative final height was found to be equal to a when $a \lesssim 2$ and to $a^{0.45}$ when $a \gtrsim 2$, while the rescaled run-out distance $\Delta L_f/L_0$ was equal to a when $a \lesssim 2$ and to $1.3 a^{0.7}$ when $a \gtrsim 2$. These expressions give results of the same level of accuracy as Eqs. (10a), (10b), (11a), and (11b) for the data at low release velocity, in the range of explored aspect ratios.

C. Influence of the release velocity

The previous subsections characterized the two limiting cases of the free-fall and the quasistatic regimes, considering a sufficiently high or low velocity of the sliding gate, respectively. A transition is expected between these two asymptotic behaviors, where the release velocity V has still an impact on the collapse dynamics, and in particular on the velocity of the granular front v_f at the base of the column.

To finely study the influence of the sliding gate, we compare the mean value of the release velocity \bar{V} , integrated over the time during which the gate is in contact with the grains, to the mean velocity \bar{v}_f of the advancing granular front taken at the foot of the column, i.e., at $z = d$. The value of \bar{v}_f is determined here as done by Lajeunesse *et al.* [4], i.e., by taking the tangent of the run-out distance as a function of time within the region of nearly constant velocity, as illustrated in Fig. 9(a) for an intermediate release velocity (nominal value $V = 0.2 \text{ m s}^{-1}$, mean value $\bar{V} \simeq 0.19 \text{ m s}^{-1}$). Even though the acceleration stage of the granular front at high release velocities was found to be quadratic in time in Sec. IV A, this is not the case for the quasistatic regime. Indeed, for low release velocities, the advancing front is roughly triangular, with a shape dictated by the angle of repose of the material. Hence, the definition of the mean front velocity \bar{v}_f gives a more general indication of the collapse dynamics for the present discussion.

In Fig. 9(b), we report for all data of series C–E the evolution of \bar{v}_f as a function of \bar{V} , both normalized by the typical

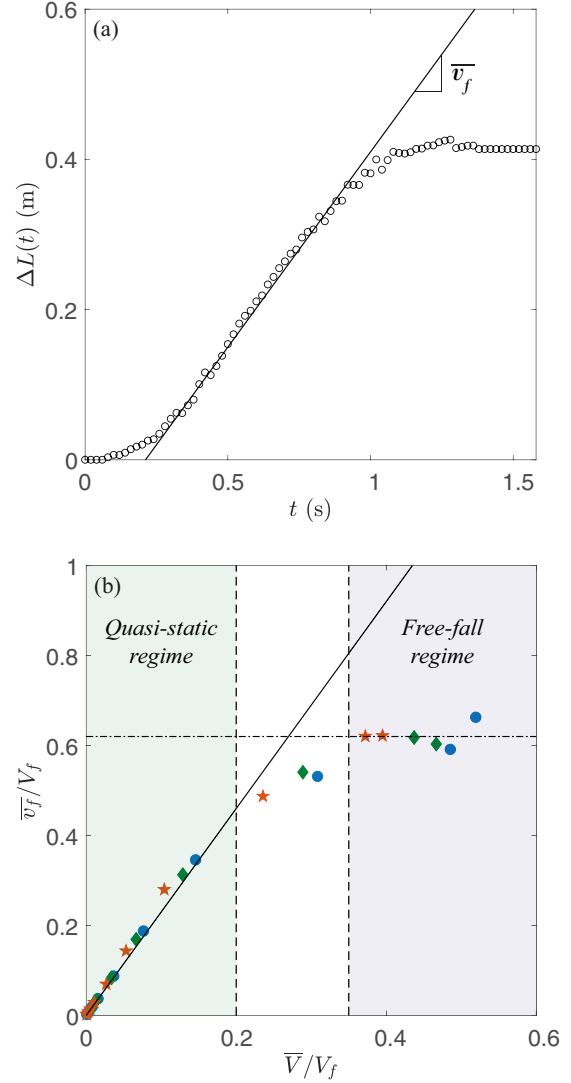


FIG. 9. (a) Time evolution of the run out of a column with $H_0 = 37.5 \text{ cm}$, $L_0 = 7.5 \text{ cm}$ ($a = 5$), with a release velocity of 0.2 m s^{-1} ; (—) estimation of the mean front velocity, with a slope $\bar{v}_f = 0.52 \text{ m s}^{-1}$ in this case. (b) Evolution of the front velocity \bar{v}_f with the mean release velocity \bar{V} , both nondimensionalized by V_f , which is given by Eq. (13). (●) $a = 0.75$; (◆) $a = 2$; and (★) $a = 5$. The horizontal dash-dotted line shows the plateau value $\bar{v}_f/V_f = 0.62$. The continuous line corresponds to Eq. (15) with $\theta_r = 23.5^\circ$. The vertical dashed lines highlight the values $\bar{V}/V_f \simeq 0.2$ marking the limit of the quasistatic regime, and $\bar{V}/V_f \simeq 0.35$ above which no significant influence of the release velocity is observed.

advancing front velocity V_f of the free-fall regime,

$$V_f = \sqrt{2\bar{\beta}g\Delta L_f} \simeq \begin{cases} 0.74 \sqrt{2gH_0} & \text{for } a \lesssim 3, \\ 0.89 a^{-1/6} \sqrt{2gH_0} & \text{for } a \gtrsim 3, \end{cases} \quad (13)$$

where $\bar{\beta} \simeq 0.30$. The release velocity was varied over three decades in these experiments, for three representative initial aspect ratios of 0.75 (●), 2 (◆), and 5 (★), respectively.

All data collapse well onto a master curve, showing the same behavior at all considered aspect ratios. For $\bar{V}/V_f \lesssim 0.2$, the velocity of the advancing granular front \bar{v}_f is governed by

the release velocity, and a quasistatic evolution is observed for the granular slide. As discussed in Sec. III, in this case, the moving interface exhibits at leading order a triangular shape dictated by the angle of repose of the material. Hence, during the spreading of the column, the run-out distance, which can be approximated by $\Delta L(0, t) \simeq \bar{v}_f t$ as illustrated in Fig. 9(a), is related to the distance $z_g(t) \simeq \bar{V} t$ from the bottom plane to the bottom of the gate through the relation

$$\Delta L(0, t) \simeq \frac{z_g(t)}{\tan \theta_r}, \quad (14)$$

which, by taking the time derivative of each terms, gives the following relation between \bar{v}_f and \bar{V}

$$\bar{v}_f \simeq \frac{\bar{V}}{\tan \theta_r}. \quad (15)$$

This relation is represented by the continuous line in Fig. 9(b), which fits well the experiments at low release velocity ($\bar{V}/V_f \lesssim 0.2$), with $\theta_r = 23.5^\circ$. When $\bar{V}/V_f \gtrsim 0.35$, \bar{v}_f/V_f saturates at a constant value of about 0.62 ± 0.05 . Therefore, the value of \bar{V} does not influence the granular collapse dynamics anymore, which corresponds to the free-fall regime. Combining this plateau value of 0.62 with Eq. (15), the transition between these two asymptotic regimes is expected around $\bar{V} \simeq 0.62 \tan \theta_r V_f \simeq 0.3 V_f$. The saturation is clearly observed when $\bar{V}/V_f \gtrsim 0.35$, which gives a condition to prevent any significant effects of the release velocity on the collapse dynamics. Indeed, for the material used in the present study, namely spherical glass beads, a conservative criterion using Eq. (13) would read

$$\bar{V} \geq \gamma \sqrt{gH_0} \quad (16)$$

with $\gamma \simeq 0.4$. The coefficient γ may slightly depend on the characteristics of the material considered, for instance, the angle of repose of the granular medium, but is independent of the aspect ratio of the initial column.

V. CONCLUSION

In the present paper, we report experimental results on the collapse of a dry granular column, where the velocity at which the grains are released is controlled. The aim was to get insights into the collapse dynamics and its influence on classical parameters such as the final height or the run-out distance of the final deposit. The release velocity was varied over three decades, for several initial aspect ratios of the column. Different regimes for the collapse were identified depending on the release velocity V .

For large values of V , classical power laws are recovered for H_f and ΔL_f as a function of the initial aspect ratio a [4]. In this regime, the deposits exhibit a significant curvature. For sufficiently high aspect ratios ($a \gtrsim 3$), the top of the granular column undergoes an overall free-fall-like motion at a typical

acceleration smaller than gravity, of about 0.5g, followed by a deceleration to the final state. During the spreading of the collapsing column, the grains moving horizontally also experience a free-fall-like motion with a smaller acceleration, of about 0.3g, followed by a deceleration stage leading to the final state of the deposits. By focusing on the bottom of the column, the duration of the granular collapse is found to either be constant at $a \lesssim 3$ or to slightly depend on the aspect ratio of the column when $a \gtrsim 3$, through a power law of exponent $-1/6$. This result explains the behavior reported in Ref. [14].

At low release velocities, a quasistatic evolution for the collapse is observed, where the motion is mainly controlled by the angle of repose of the material. In this case, the final shape of the deposits is triangular for sufficiently high aspect ratios ($a \gtrsim 0.9$), and trapezoidal otherwise ($a \lesssim 0.9$), as part of the column remains strictly static. Based on these observations and using the conservation of mass, expressions for the final height H_f and run-out distance ΔL_f as a function of a are derived, and the critical aspect ratio a_c separating the triangular and the trapezoidal shapes is found to depend only on the angle of repose of the material. These scalings are found to be identical to those obtained for the viscous regime of the collapse of immersed granular columns [26], and quantitatively match the empirical scalings of Mériaux [10]. In that respect, they seem to be characteristic of a quasistatic granular collapse, occurring once inertia is negligible.

Between these two asymptotic regimes at high and low release velocities, a transition exists, where an increasing release velocity has a decreasing influence on the collapse dynamics. In the present study, no more effect of the mean release velocity \bar{V} on the collapse dynamics is observed as soon as $\bar{V} \gtrsim 0.35 V_f$, where V_f is the typical advancing front velocity of the free-fall regime given by Eq. (13). This relation gives a practical criterion that should be used to ensure that the release process has no influence on the collapse dynamics in future experimental works. For the present investigation, in which glass beads were used, this criterion is $\bar{V} \geq 0.4 \sqrt{gH_0}$.

In this study, we focused on quasi-two-dimensional granular collapses. However, it would be interesting to compare these results to the axisymmetric case, where different scalings govern the final morphology of the deposit [3]. Besides, such a configuration is more realistic for describing large geophysical flows such as landslides, which are a threat for human facilities both in mountainous and coastal areas, as landslides entering into water are known for their tsunamigenic potential [36–40].

ACKNOWLEDGMENTS

The authors are grateful to J. Amarni, A. Aubertin, L. Auffray, and R. Pidoux for the elaboration of the experimental setup. The authors report no conflict of interest.

[1] V. J. Langlois, A. Quiquerez, and P. Allemand, Collapse of a two-dimensional brittle granular column: Implications for understanding dynamic rock fragmentation in a landslide, *J. Geophys. Res. Earth. Surf.* **120**, 1866 (2015).

[2] E. Lajeunesse, C. Quantin, P. Allemand, and C. Delacourt, New insights on the runout of large landslides in the Valles-Marineris canyons, Mars, *Geophys. Res. Lett.* **33**, L04403 (2006).

- [3] E. Lajeunesse, A. Mangeney-Castelnau, and J. P. Vilotte, Spreading of a granular mass on a horizontal plane, *Phys. Fluids* **16**, 2371 (2004).
- [4] E. Lajeunesse, J. Monnier, and G. Homsy, Granular slumping on a horizontal surface, *Phys. Fluids* **17**, 103302 (2005).
- [5] G. Lube, H. E. Huppert, R. S. J. Sparks, and M. A. Hallworth, Axisymmetric collapses of granular columns, *J. Fluid Mech.* **508**, 175 (2004).
- [6] G. Lube, H. E. Huppert, R. S. J. Sparks, and A. Freundt, Collapses of two-dimensional granular columns, *Phys. Rev. E* **72**, 041301 (2005).
- [7] L. Staron and E. Hinch, Study of the collapse of granular columns using two-dimensional discrete-grain simulation, *J. Fluid Mech.* **545**, 1 (2005).
- [8] N. J. Balmforth and R. R. Kerswell, Granular collapse in two dimensions, *J. Fluid Mech.* **538**, 399 (2005).
- [9] R. Zenit, Computer simulations of the collapse of a granular column, *Phys. Fluids* **17**, 031703 (2005).
- [10] C. Mériaux, Two dimensional fall of granular columns controlled by slow horizontal withdrawal of a retaining wall, *Phys. Fluids* **18**, 093301 (2006).
- [11] E. Larrieu, L. Staron, and E. J. Hinch, Raining into shallow water as a description of the collapse of a column of grains, *J. Fluid Mech.* **554**, 259 (2006).
- [12] L. Staron and E. J. Hinch, The spreading of a granular mass: Role of grain properties and initial conditions, *Granular Matter* **9**, 205 (2007).
- [13] E. L. Thompson and H. E. Huppert, Granular column collapses: Further experimental results, *J. Fluid Mech.* **575**, 177 (2007).
- [14] L. Lacaze, J. C. Phillips, and R. R. Kerswell, Planar collapse of a granular column: Experiments and discrete element simulations, *Phys. Fluids* **20**, 063302 (2008).
- [15] M. Trepanier and S. V. Franklin, Column collapse of granular rods, *Phys. Rev. E* **82**, 011308 (2010).
- [16] P.-Y. Lagrée, L. Staron, and S. Popinet, The granular column collapse as a continuum: Validity of a two-dimensional Navier-Stokes model with a $\mu(I)$ -rheology, *J. Fluid Mech.* **686**, 378 (2011).
- [17] L. Rondon, O. Pouliquen, and P. Aussillous, Granular collapse in a fluid: Role of the initial volume fraction, *Phys. Fluids* **23**, 073301 (2011).
- [18] H. Tapia-McClung and R. Zenit, Computer simulations of the collapse of columns formed by elongated grains, *Phys. Rev. E* **85**, 061304 (2012).
- [19] V. Topin, Y. Monerie, F. Perales, and F. Radjai, Collapse Dynamics and Runout of Dense Granular Materials in a Fluid, *Phys. Rev. Lett.* **109**, 188001 (2012).
- [20] R. Artoni, A. C. Santomaso, F. Gabrieli, D. Tono, and S. Cola, Collapse of quasi-two-dimensional wet granular columns, *Phys. Rev. E* **87**, 032205 (2013).
- [21] M. Degaetano, L. Lacaze, and J. C. Phillips, The influence of localised size reorganisation on short-duration bidispersed granular flows, *Eur. Phys. J. E* **36**, 36 (2013).
- [22] J. M. Warnett, P. Denissenko, P. J. Thomas, E. Kiraci, and M. A. Williams, Scalings of axisymmetric granular column collapse, *Granular Matter* **16**, 115 (2014).
- [23] P. Mutabaruka, K. Kumar, K. Soga, F. Radjai, and J.-Y. Delenne, Transient dynamics of a 2D granular pile, *Eur. Phys. J. E* **38**, 47 (2015).
- [24] I. R. Ionescu, A. Mangeney, F. Bouchut, and O. Roche, Viscoplastic modeling of granular column collapse with pressure-dependent rheology, *J. Nonnewton. Fluid Mech.* **219**, 1 (2015).
- [25] L. Jing, G. C. Yang, C. Y. Kwok, and Y. D. Sobral, Dynamics and scaling laws of underwater granular collapse with varying aspect ratios, *Phys. Rev. E* **98**, 042901 (2018).
- [26] A. Bougouin and L. Lacaze, Granular collapse in a fluid: Different flow regimes for an initially dense-packing, *Phys. Rev. Fluids* **3**, 064305 (2018).
- [27] M. Cabrera and N. Estrada, Granular column collapse: Analysis of grain-size effects, *Phys. Rev. E* **99**, 012905 (2019).
- [28] M. Ordaz, M. Sánchez-Rosas, J. Hernández-Juárez, A. Medina, and D. Serrano, Collapse of conical granular columns, *EPJ Web Conf.* **249**, 03013 (2021).
- [29] T. Man, H. E. Huppert, L. Li, and S. A. Galindo-Torres, Deposition morphology of granular column collapses, *Granular Matter* **23**, 59 (2021).
- [30] Y. Sun, W. Zhang, Y. An, Q. Liu, and X. Wang, Experimental investigation of immersed granular collapse in viscous and inertial regimes, *Phys. Fluids* **33**, 103317 (2021).
- [31] G. C. Yang, L. Jing, C. Y. Kwok, and Y. D. Sobral, Size effects in underwater granular collapses: Experiments and coupled lattice Boltzmann and discrete element method simulations, *Phys. Rev. Fluids* **6**, 114302 (2021).
- [32] P. Jop, Y. Forterre, and O. Pouliquen, A constitutive law for dense granular flows, *Nature (London)* **441**, 727 (2006).
- [33] A. Sauret, N. Balmforth, C. Caulfield, and J. McElwaine, Bulldozing of granular material, *J. Fluid Mech.* **748**, 143 (2014).
- [34] S. Courrech du Pont, P. Gondret, B. Perrin, and M. Rabaud, Wall effects on granular heap stability, *EPL* **61**, 492 (2003).
- [35] M. Robbe-Saule, Modélisation expérimentale de génération de tsunami par effondrement granulaire, Ph.D. thesis, Université Paris Saclay, 2019, <https://tel.archives-ouvertes.fr/tel-02459774>.
- [36] B. Huang, Q. Zhang, J. Wang, C. Luo, X. Chen, and L. Chen, Experimental study on impulse waves generated by gravitational collapse of rectangular granular piles, *Phys. Fluids* **32**, 033301 (2020).
- [37] M. A. Cabrera, G. Pinzon, W. A. Take, and R. P. Mulligan, Wave generation across a continuum of landslide conditions from the collapse of partially submerged to fully submerged granular columns, *J. Geophys. Res. [Oceans]* **125**, e2020JC016465 (2020).
- [38] M. Robbe-Saule, C. Morize, R. Henaff, Y. Bertho, A. Sauret, and P. Gondret, Experimental investigation of tsunami waves generated by granular collapse into water, *J. Fluid Mech.* **907**, A11 (2021).
- [39] M. Robbe-Saule, C. Morize, Y. Bertho, A. Sauret, A. Hildenbrand, and P. Gondret, From laboratory experiments to geophysical tsunamis generated by subaerial landslides, *Sci. Rep.* **11**, 18437 (2021).
- [40] W. Sarlin, C. Morize, A. Sauret, and P. Gondret, Nonlinear regimes of tsunami waves generated by a granular collapse, *J. Fluid Mech.* **919**, R6 (2021).